Proceedings of the 4th ITB Graduate School Conference
Innovation and Discovery for Sustainability
July 6, 2023

Preparation and Characterization of Palladium-based/α-Alumina Membrane by Electroless Plating

Raihan Annisa Fitri[1], Andapeng[2], Tatsuya Suzuki[2], Torazawa Makoto[2], Hafis Pratama Rendra Graha[1], Yulia Tri Rahkadima[1], Elvi Restiawaty[3,4], Manabu Miyamoto[2], Shigeyuki Uemiya[2] & Yogi Wibisono Budhi[1,4,5,*]

[1]Department of Chemical Engineering, Faculty of Industrial Technology, Institut Teknologi Bandung, Jalan Ganesha 10 Bandung 40132, Indonesia
[2]Department of Chemistry and Biomolecular Science, Faculty of Engineering, Gifu University, 1-1 Yanagido, Gifu 501-1193, Japan
[3]Department of Bioenergy Engineering and Chemurgy, Faculty of Industrial Technology, Institut Teknologi Bandung, Jalan Let. Jend. Purn. Dr. (HC) Mashudi No.1, Sumedang 45363, Indonesia
[4]Research Group of Chemical Engineering Process Design and Development, Faculty of Industrial Technology, Institut Teknologi Bandung, Jalan Ganesha 10, Bandung 40132, Indonesia
[5]Research Center for Nanoscience and Nanotechnology, Institut Teknologi Bandung, Jalan Ganesha 10 Bandung 40132, Indonesia
*Email: y.wibisono@itb.ac.id

Abstract. Palladium (Pd) membranes have been prepared by the electroless plating (ELP) method using hydrazine monohydrate (N2H4·H2O) as a reducing agent onto tubular porous alumina (α-Al2O3) supports. In this work, four Pd/α-Al2O3 membranes (M1–M4) were fabricated under different plating repetitions. Electroless plating was carried out at 50 °C for 90 minutes each time. This study aims to investigate the morphology of membranes of different thicknesses. The membrane turned into characterized by using Scanning Electron Microscopy (SEM), Atomic Force Microscope (AFM), and X-ray diffraction (XRD). Scanning electron microscopy images display that the synthesized thicknesses are from 10.25 to 22.53 µm. Atomic Force Microscopy (AFM) reveals a relation between the roughness and the thickness, and the roughness increases as the thickness increases. X-ray diffraction studies imply that the synthesized M1 has a face-centered cubic phase (FCC), with an average crystallites size of 12.35 nm for M1 while 12.62 nm, 18.67 nm and 26.12 nm for M2, M3 and M4, respectively.

Keywords: *crystallite; electroless plating; face-centered cubic; morphology; Pd/α-Al2O3 membrane; roughness; thickness.*

1 Introduction

In the chemical processing sector as well as in mobile and stationary fuel cell applications, Pd membranes have the potential to use energy more effectively. Given the growing international pressure on non-renewable resources, it is crucial to minimize the environmental effects of energy production and consumption [1].

Metal composite membranes, especially Pd-based membranes, are widely used for hydrogen separation because they have good permeability and selectivity to hydrogen and can be operated at high temperatures [2]–[4]. The palladium layer thickness and membrane cost can be significantly reduced with composite membranes with porous supports while ensuring increased permeability and reliable performance [5].

Palladium has a high hydrogen permselectivity, which led to the development of palladium membranes. Due to the intense surface interaction between hydrogen and palladium, this characteristic is produced. It first causes the formation of a solid hydrogen solution in palladium (α phase) and a hydride (β phase) at higher hydrogen concentrations. However, there are significant disadvantages, including the cost and the potential for the palladium layer to become embrittlement. This is primarily due to the phase transition from the α phase to the hybrid β phase at low temperatures in the presence of hydrogen [6].

Porous alumina ceramics have attracted much attention because they have great potential for industrial applications such as heat insulators, gas separation, and catalyst supports [7]. A porous alumina ceramic membrane tube is mainly chosen as the substrate due to its high alumina purity, which leads to high chemical stability in acid, base, and other reactive environments and high thermal and hydrothermal stability [8], [9].

Electroless plating occurs through an autocatalytic reaction mechanism initiated by an activated surface. Prior to plating, the substrate is activated by scattering Pd nuclei across its surface. These sites start the electroless plating reaction by catalyzing hydrazine decomposition in the plating bath. Electroless plating can be implemented for non-conductive materials such as plastics, glasses, ceramics, and semiconductors and does not require an anode. This method is commonly used because it provides distinct advantages, such as low cost and lower deposition rates, resulting in homogeneous and smooth thin film coatings [10]. In this study, the repetition of plating using electroless plating were carried out. The morphology of the resulting membranes with different thicknesses were studied using SEM, AFM, and XRD.

2 Experimental Procedure

2.1 Materials

The material used for membranes support is α-alumina tube (α-Al_2O_3, outside diameter 10 mm, inside diameter 7 mm, and pore size 0.1 μm, NGK Insulators, Ltd.). Nitric acid (60% HNO_3, Nacalai Tesque) and ultrapure water were used to wash the membranes. Chemicals that produce sensitizing solutions include

stannous chloride (97.0% $SnCl_2 \cdot 2H_2O$, Nacalai Tesque) and hydrochloric acid (35% HCl, Nacalai Tesque. The activation solution consisted of palladium chloride (100.00% $PdCl_2$, Tanaka Kikinzoku Kogyo Co., Ltd.) and hydrochloric acid (35% HCl, Nacalai Tesque). The solution used for the electroless plating contained tetraamine palladium dichloride (41,34% TAPDC, Tanaka Kikinzoku Kogyo Co., Ltd.), hydrazine monohydrate (98% $N_2H_4 \cdot H_2O$, Nacalai Tesque), di-sodium dihydrogen ethylenediamine tetraacetate dihydrate (99,5% $Na_2EDTA \cdot 2H_2O$, Nacalai Tesque), and ammonia solution (28% NH_3, Nacalai Tesque).

2.2 Membrane Preparation

Synthesis of the Pd/α-Al_2O_3 membrane was accomplished through several steps, including cleaning the membranes, sensitizing and activating the membrane, and coating using the electroless plating method. Nitric acid and ultrapure water were used in an ultrasonic bath to clean the membrane. Then the membrane was dried in a furnace to remove all cleaning agents from its pore. After that, the membrane was dipped in a sensitization solution consisting of $SnCl_2$ and HCl, then washed with ultrapure water. The membrane was then dipped into the activation solution of $PdCl_2$ and HCl. The membrane was rewashed with ultrapure water. Before beginning the electroless plating process, this process is repeated to produce sufficient Pd nucleus on the surface of the membrane support. Table 1 displays the composition of Pd electroless plating. The membrane was washed with ultrapure water and heated in an oven.

Table 1 Composition of Pd electroless plating bath.

Component	Pd bath
TAPDC (g/L)	5.40
$Na_2EDTA \cdot 2H_2O$ (g/L)	67.20
Aqueous NH_3 (mL/L)	650.67
Aqueous $N_2H_4 \cdot H_2O$ (mL/L)	2.00
Temperature (°C)	50.00

2.3 Membrane Characterization

The surface morphology of the Pd layer was observed by Scanning Electron Microscopy (SEM, S-4800, Hitachi) equipped with an Atomic Force Microscope (AFM5400L, Hitachi) where no coating was required. X-Ray Diffraction patterns (XRD, D8 Advance, Bruker) with a nickel filter were used to determine the crystal structure of the Pd films. The voltage was set at 40 kV and the current at 40 mA.

3 Results and Discussion

3.1 Scanning Electron Microscopy (SEM)

The thickness of the palladium film depends on the number of plating repetitions. Figure 1 shows the thickness of the palladium and α-alumina layers on a two-layer cross-section of the palladium-alumina composite membrane for each plating repetition (plating time 90 minutes for each plating repetition).

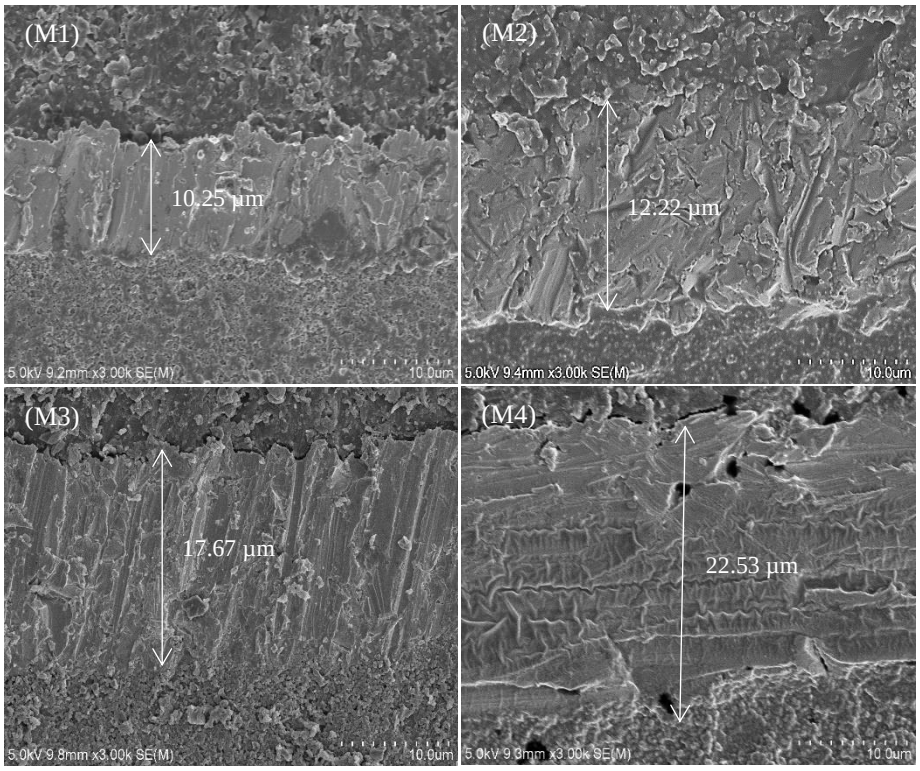

Figure 1 SEM image of Pd/α-Al_2O_3.

The palladium film covers the α-alumina layer. Due to the homogeneous distribution of palladium nuclei during the activation process, the reaction process proceeds uniformly across the surface of the α-alumina. Palladium film and nucleus growth take place concurrently during this process. As shown in Figure 1, the palladium film thickness rises proportionally as the plating time increases (from 2 plating repetitions to 5 plating repetitions). Palladium can be formed by a reduction mechanism with a reducing agent. In electroless palladium plating in hydrazine-based baths, the redox reaction can be represented as follows:

Reduction reaction:

$$Pd(complex)^{2+} + 2e^- \rightarrow Pd^0 \quad (1)$$

Oxidation reaction:

$$N_2H_4 + 4OH^- \rightarrow N_2 + 4H_2O + 4e^- \quad (2)$$

Overall reaction:

$$2Pd^{2+} + N_2H_4 + 4OH^- \rightarrow N_2 + 4H_2O + Pd^0 \quad (3)$$

The electrons released during the reaction are used to decompose the palladium complex to palladium, with the rate of deposition increasing with the number of available palladium sites [11]. The presence of palladium is evidenced by the XRD analysis shown in Figure 2.

3.2 X-Ray Diffraction (XRD)

The phase purity and crystallinity of M1–M4 were investigated by X-ray Diffraction over a 2θ range of 30º–90º. Figure 2 displays the diffraction pattern of the Pd membrane. Five peaks of Pd at 2θ = 39.90º, 46.53º, 67.94º, 81.98º and 86.39º, which correspond to (111), (200), (220), (311), and (222) crystalline planes of Pd. All the diffraction peaks of the XRD pattern (Figure 2) could be indexed to the face-centered cubic (FCC) phase of palladium (JCPDS card No. 05-0681) [12]. The crystallinity index (CI) is calculated using the method reported by Pardo et al. [13].

$$CI = \frac{A_c}{A_c + A_a} \quad (4)$$

The crystallinity index of M1–M4 decreased from 69.61 to 30.56 % by increasing the film thickness (Table 2). Same phenomena was observed by Alkatun [14]. The average crystallite sizes of the obtained Pd film were calculated using the Scherrer equation [15].

$$D_{hkl} = \frac{K\lambda}{\beta cos\theta_{hkl}} \quad (5)$$

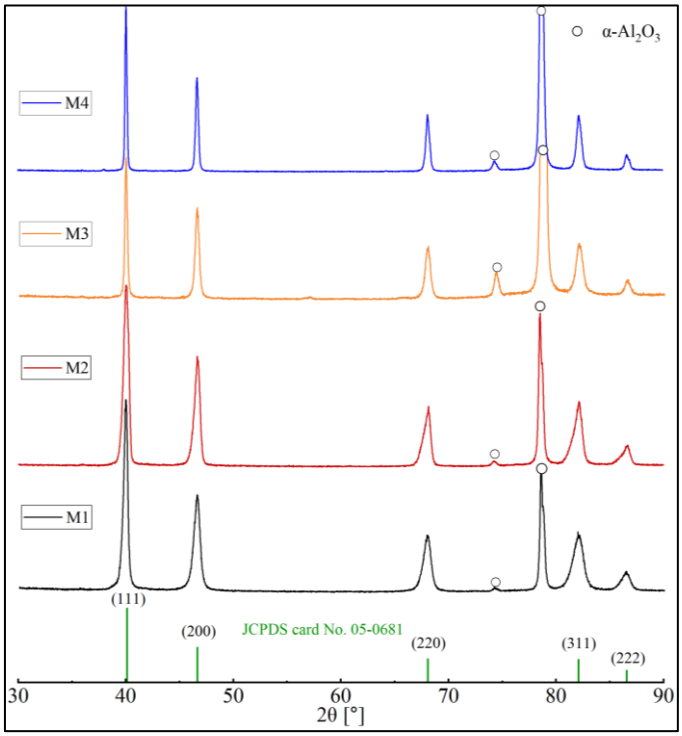

Figure 2 The XRD pattern of Pd membrane.

The average crystallite size calculated for M1–M4 were found to be 12.35–26.12 nm as shown in Table 2. This shows that as thickness increases, the average crystallite size grows [16]. The strain and dislocation density of the material are other important factors that can be calculated from XRD data [17]. The strain (ε) and dislocation density (δ) values for all the samples were calculated using the following relations and tabulated in Table 2. As shown in Table 2, the dislocation density and strain values decrease with increasing film thickness [14], from 7.55 × 10^{-3} to 1.82 × 10^{-3} (nm^{-2}) and from 5.99 × 10^{-3} to 2.84 × 10^{-3}, respectively.

$$\varepsilon = \frac{\beta \times cos\theta}{4} \tag{6}$$

$$\delta = \frac{15 \times \varepsilon}{a \times D} \tag{7}$$

Table 2 Crystallinity index (CI), lattice constants, crystallites sizes (D), dislocation density (δ) and strain (ε) of Pd membrane (M1–M4).

Membrane	Thickness (μm)	CI (%)	Lattice constant (Å)	D (nm)	δ x 10^{-3} (nm^{-2})	ε x 10^{-3}
M1	10.25	69.6	3.901	12.350	7.546	5.988
M2	12.22	67.02	3.896	12.615	6.618	5.757
M3	17.67	42.26	3.897	18.686	3.971	4.083
M3	22.53	30.56	3.888	26.122	1.819	2.841

3.3 Atomic Force Microscope (AFM)

AFM contact mode was utilized to study the morphology of Pd films. Figure 3 displays various 3D AFM images of the samples obtained at different thicknesses. The samples were scanned in an area of 50 μm x 50 μm. The microscopic images of the samples reveal little homogeneous surfaces and their roughness increases with increasing thickness.

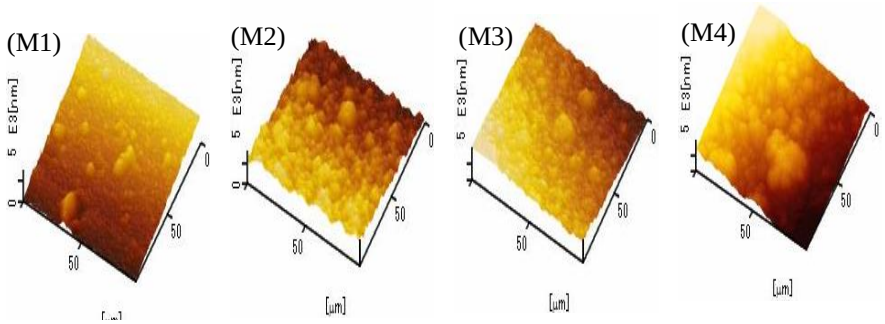

Figure 3 AFM images of the skin layer surface of Pd/α-Al_2O_3.

Figure 3 shows the morphological differences in palladium films as the thickness varied. The brightest areas in these images represent the membrane's highest point, while the darkest areas represent valleys or membrane pores. The correlation between roughness, grain size, and thickness variation is shown in Table 3.

Table 3 The correlation between the roughness and grain size of Pd film with the plating time of 90 minutes for each repetition.

Membrane	Number of plating repetitions	Thickness (µm)	Roughness (µm)	Grain Size (µm)
M1	2	10.25	1.66	7.18
M2	3	12.22	1.76	8.30
M3	4	17.67	2.10	9.25
M4	5	22.53	2.54	11.78

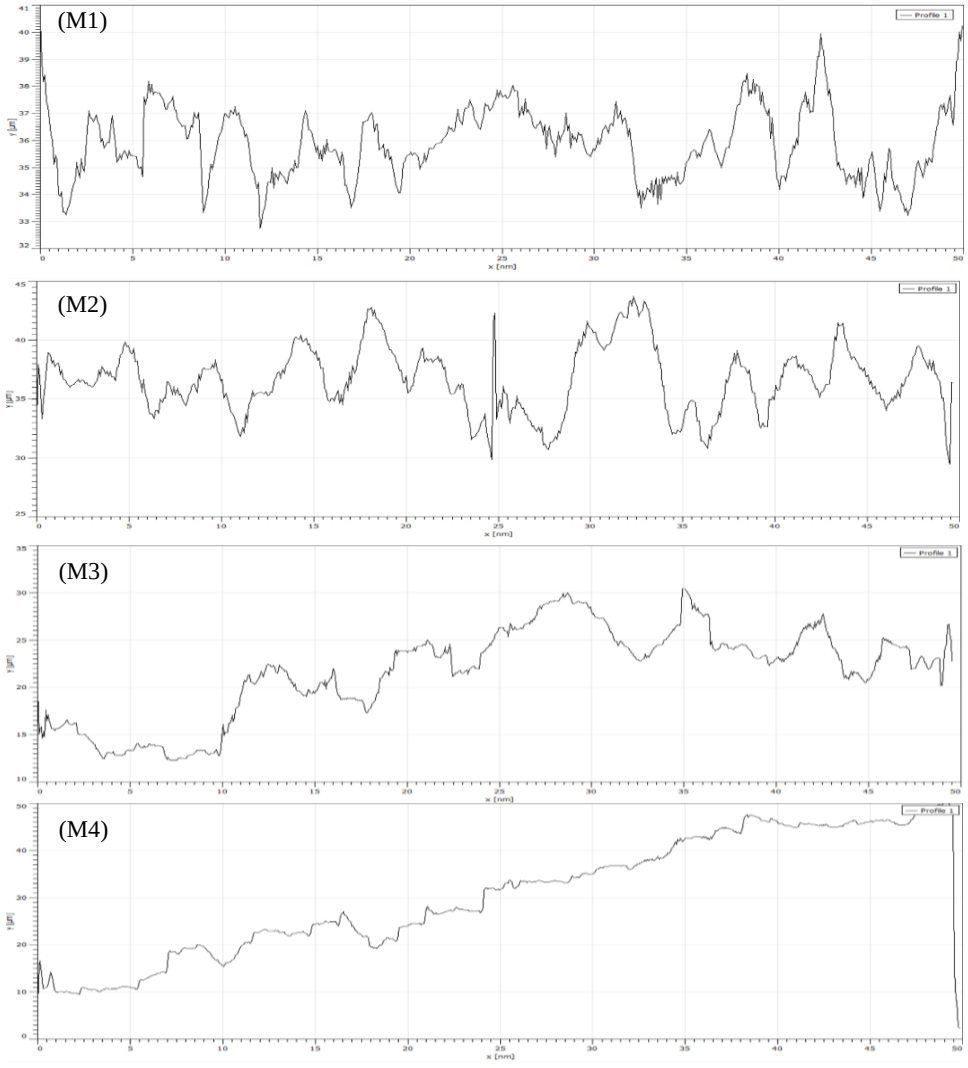

Figure 4 Texture profiles of AFM images of palladium films.

According to Table 3, the grain size grows as the film thickness increases. Additionally, a number of other parameters, including as the substrate's material, temperature, magnetron size, and external substrate heating during the deposition, affect the grain size [18]. With a root mean square roughness (Rq) of 1.66 m, the sample grown at M1 has the most homogeneous surface. The roughness of the surface of the sample grown at M2 and M3 is (Rq = 1.76 m) and (Rq = 2.10 m), respectively. The sample grown at M4 has the surface with the highest roughness (Rq = 2.54 m) and columnar growth. The texture profile of the cross-section area of the AFM images, obtained by the Gwyddion software, obtained the grain size of Pd films statistically, and shown in Figure 4, confirms that the surfaces of the sample grown at M1 and M2 have smaller grain sizes than the surfaces of the sample grown at M3 and M4.

4 Conclusion

Pd/α-Al_2O_3 were prepared using the electroless plating method with varying plating repetitions (M1–M4). SEM analysis showed the thickness obtained were 10.25 µm, 12.22 µm, 17.67 µm, and 22.53 µm. AFM studies indicate that the Pd's surface roughness and grain size increased as the thickness increased, from 7.18 to 11.78 µm. The XRD analysis confirmed the face-centered cubic (FCC) phase of palladium and has an average lattice constant of 3.89 Å. The XRD analysis also obtained the crystallite size of 12.35–26.12 nm and the crystallinity index of 69.61–30.56%.

Acknowledgment

This work was supported by the Indonesia endowment fund for education (LPDP), the Ministry of Finance of Indonesia [grant number RISPRO/KI/BI/KOM/II/ 16507/I/2020]. The authors also thank Institut Teknologi Bandung, Department of Chemistry and Biomolecular Science, Faculty of Engineering, Gifu University, for supporting this research and Japan Student Services Organization (JASSO) for providing scholarships.

Nomenclature

A	=	Lattice constant
A_a	=	Area of amorphous hollows
A_c	=	Area under crystalline peaks
B	=	Full-width half-maximum (FWHM)
D	=	Crystallites size
E	=	Strain
Hkl	=	Denotes the diffraction plane (Bravais lattice)

K = Scherrer constant, taken as 0.9
Λ = Wavelength of the X-ray sources
Δ = Dislocation density
Θ = Peak position

References

[1] S. N. Paglieri, K. Y. Foo, J. D. Way, J. P. Collins, and D. L. Harper-Nixon, "A New Preparation Technique for Pd/Alumina Membranes with Enhanced High-Temperature Stability," *Ind. Eng. Chem. Res.*, vol. 38, no. 5, pp. 1925–1936, May 1999, doi: 10.1021/ie980199c.

[2] A. Basile and F. Gallucci, "Final Remarks," in *Membranes for Membrane Reactors*, John Wiley & Sons, Ltd, 2011, pp. 591–597. doi: https://doi.org/10.1002/9780470977569.oth1.

[3] K. Zhang and J. D. Way, "Palladium-copper membranes for hydrogen separation," *Separation and Purification Technology*, vol. 186, pp. 39–44, 2017, doi: https://doi.org/10.1016/j.seppur.2017.05.039.

[4] G. S. Burkhanov, N. B. Gorina, N. B. Kolchugina, N. R. Roshan, D. I. Slovetsky, and E. M. Chistov, "Palladium-Based Alloy Membranes for Separation of High Purity Hydrogen from Hydrogen-Containing Gas Mixtures," *Platinum Metals Review*, vol. 55, pp. 3–12, 2011, doi: https://doi.org/10.1595/147106711X540346.

[5] R. Sari, Z. Yaakob, M. Ismail, and W. Wan Daud, "Preparation of Palladium-Alumina Membrane Tube by Combine Sol-gel Process with Electroless Plating for Hydrogen Permeation," *Journal of Applied Sciences*, vol. 10, no. 12, pp. 1151–1156, Dec. 2010, doi: 10.3923/jas.2010.1151.1156.

[6] S. Yun, "Fabrication of Ultrathin Palladium Composite Membranes by a New Technique and Their Application in the Ethanol Steam Reforming for H_2 Production," Faculty of the Virginia Polytechnic Institute and State University, Ph.D. dissertation, 2011. [Online]. Available: https://vtechworks.lib.vt.edu/handle/10919/37505

[7] B. Dong, G. Wang, B. Yuan, J. Han, K. Chen, and H. Li, "Fabrication and properties of porous alumina ceramics with three different pore sizes," *Journal of Porous Materials*, vol. 24, no. 3, pp. 805–811, Jun. 2017, doi: 10.1007/s10934-016-0319-4.

[8] B. Ernst, S. Haag, and M. Burgard, "Permselectivity of a nickel/ceramic composite membrane at elevated temperatures: A new prospect in hydrogen separation?," *Journal of Membrane Science*, vol. 288, no. 1, pp. 208–217, Feb. 2007, doi: https://doi.org/10.1016/j.memsci.2006.11.017.

[9] H. Bissett, J. Zah, and H. M. Krieg, "Manufacture and optimization of tubular ceramic membrane supports," *Powder Technology*, vol. 181, no. 1, pp. 57–66, Jan. 2008, doi: https://doi.org/10.1016/j.powtec.2007.06.005.

[10] N. Eliaz and E. Gileadi, *Physical Electrochemistry: Fundamentals, Techniques, and Applications*, 2nd ed. Wiley, 2019.

[11] A. Alkali, "Electroless Plating of Palladium Membranes on Porous Substrates for Hydrogen Separation and the Effects of Process Factors on Plating Rate and Efficiency: A Review," *Journal of Power and Energy Engineering*, vol. 8, no. 2, pp. 1–19, Feb. 2020, doi: https://doi.org/10.4236/jpee.2020.82001.

[12] R. Mostafalu, A. Heydari, A. Banaei, F. Ghorbani, and M. Arefi, "The use of palladium nanoparticles supported on active carbon for synthesis of disproportionate rosin (DPR)," *Journal of Nanostructure in Chemistry*, vol. 7, no. 1, pp. 61–66, Mar. 2017, doi: 10.1007/s40097-017-0220-y.

[13] F. N. Pardo, G. M. Barrera, A. L. M. Hernández, V. M. Castaño, J. L. R. Aementa, F. M. Rodríguez, and C. V. Santos, "Effects on the Thermo-Mechanical and Crystallinity Properties of Nylon 6,6 Electrospun Fibres Reinforced with One Dimensional (1D) and Two Dimensional (2D) Carbon," *Materials*, vol. 6, no. 8, pp. 3494–3513, Aug. 2013, doi: https://doi.org/10.3390/ma6083494.

[14] Y. Akaltun, "Effect of thickness on the structural and optical properties of CuO thin films grown by successive ionic layer adsorption and reaction," *Thin Solid Films*, vol. 594, pp. 30–34, Nov. 2015, doi: https://doi.org/10.1016/j.tsf.2015.10.003.

[15] W.-H. Lin and H.-F. Chang, "Characterizations of Pd–Ag membrane prepared by sequential electroless deposition," *Surface and Coatings Technology*, vol. 194, no. 1, pp. 157–166, Apr. 2005, doi: https://doi.org/10.1016/j.surfcoat.2004.07.089.

[16] A. Pandey, S. Dalal, S. Dutta, and A. Dixit, "Structural characterization of polycrystalline thin films by X-ray diffraction techniques," *Journal of Materials Science: Materials in Electronics*, vol. 32, no. 2, pp. 1341–1368, Jan. 2021, doi: https://doi.org/10.1007/s10854-020-04998-w.

[17] A. Khan, A. M. Toufiq, F. Tariq, Y. Khan, R. Hussain, N. Akhtar, and S. U. Rahman, "Influence of Fe doping on the structural, optical and thermal properties of α-MnO2 nanowires," *Materials Research Express*, vol. 6, no. 6, p. 065043, Mar. 2019, doi: 10.1088/2053-1591/ab0aaf.

[18] E. Fernandez, G. J. A. Sanchez, J. L. Viviente, M. V. S. Annaland, F. Gallucci, and D. A. P. Tanaka, "Morphology and N_2 Permeance of Sputtered Pd-Ag Ultra-Thin Film Membranes," *Molecules*, vol. 21, no. 2, Feb. 2016, doi: https://doi.org/10.3390/molecules21020210.